

# Guided Lamb waves in reconfigurable phononic crystal waveguides

Cite as: APL Mater. 9, 081110 (2021); doi: 10.1063/5.0056202

Submitted: 7 May 2021 • Accepted: 28 July 2021 •

Published Online: 13 August 2021



View Online



Export Citation



CrossMark

Yan-Feng Wang,<sup>1</sup> Li Yang,<sup>2</sup> Ting-Ting Wang,<sup>3</sup> A-Li Chen,<sup>2</sup> Vincent Laude,<sup>4,a)</sup>   
and Yue-Sheng Wang<sup>1,2,a)</sup>

## AFFILIATIONS

<sup>1</sup>School of Mechanical Engineering, Tianjin University, Tianjin 300350, China

<sup>2</sup>Institute of Engineering Mechanics, Beijing Jiaotong University, Beijing 100044, China

<sup>3</sup>School of Mechanics, Civil Engineering and Architecture, Northwestern Polytechnical University, Xi'an 710129, China

<sup>4</sup>Institut FEMTO-ST, CNRS, University Bourgogne Franche-Comté, Besançon 25030, France

**Note:** This paper is part of the Special Topic on Phononic Crystals at Various Frequencies.

**a) Authors to whom correspondence should be addressed:** [vincent.laude@femto-st.fr](mailto:vincent.laude@femto-st.fr) and [yswang@tju.edu.cn](mailto:yswang@tju.edu.cn)

## ABSTRACT

We demonstrate experimentally the manipulation of Lamb waves guided along reconfigurable phononic circuits created by defects composed of threaded rods held with nuts in a perforated solid phononic crystal slab. Adjusting the free length of the rod, the resonant frequency of the defect can be tuned, without any change in the supporting phononic crystal slab. Both straight and bent waveguides are fabricated and measured in an aluminum sample with a lattice constant of 20 mm and a complete bandgap extending from 50 to 70 kHz. Guidance of Lamb waves is clearly observed by a Doppler vibrometer, even after 90° bends. The eigenmodes of guided waves are obtained using finite element analysis to explain the tuning of resonances through a bending cantilever model. Numerical and experimental results are generally found to be in fair agreement. They also suggest that the guiding frequency is rather independent of the details of the waveguides. They are of significance for the design of reconfigurable phononic devices.

© 2021 Author(s). All article content, except where otherwise noted, is licensed under a Creative Commons Attribution (CC BY) license (<http://creativecommons.org/licenses/by/4.0/>). <https://doi.org/10.1063/5.0056202>

## I. INTRODUCTION

Phononic crystals (PCs) are functional composites with spatial periodicity.<sup>1</sup> Their unique property is to exhibit bandgaps in a certain frequency range, within which propagation of elastic waves is prohibited. Thus, they have direct applications in noise isolation and vibration reduction.<sup>2</sup> When periodicity is broken, confined defect modes appear. PCs are a basis on which to design novel elastic wave devices, such as waveguides,<sup>3</sup> splitters,<sup>4</sup> or acoustic channel drop filters.<sup>5</sup> Moreover, their dispersive properties in passing bands also result in promising phenomena, such as collimation or negative refraction.<sup>6</sup>

Although PCs provide a promising pathway to the manipulation of elastic waves, they have had few real-life applications so far. Actually, most of them are characterized by a passive response and operate in fixed frequency ranges. The topology or the material parameters are hardly tunable or reconfigurable after fabrication. Tunable manipulation of acoustic or elastic waves has thus

become a fast developing topic.<sup>7</sup> Since elastic wave propagation is controlled mainly by material properties and geometry parameters,<sup>8</sup> wave manipulation can generally be classified as based on either tunability or reconfigurability.

For tunable PCs, physical or material properties are tuned using an external control field. Such PCs may be composed of multiphysical coupled components, such as piezoelectric,<sup>9–11</sup> ferroelectric,<sup>12</sup> or magnetoelastic<sup>13</sup> materials. Dynamic control can be realized by applying an external biased electric field,<sup>14,15</sup> a magnetic field,<sup>16,17</sup> and so on. Piezoelectric materials are commonly used<sup>18</sup> and can be implemented either on the surface of or inside PC units. The resonance or Bragg scattering characteristics of the periodic structure can be tuned by an external circuit so as to dynamically regulate wave propagation. When a feedback electronic control circuit is added,<sup>19</sup> active or even smart control of wave propagation can be expected. Moreover, the response can self-adapt to changes in the surrounding environment, such as an incident aerodynamic flow.<sup>20</sup>

For reconfigurable PCs, the geometry or the layout is changed in a mechanical way. For instance, tunable manipulation can be realized continuously based on the reconfigurability of fluid/solid systems: rotating or removing the solid scatterers in a fluid matrix<sup>3,21</sup> or filling a fluid in a solid matrix containing cavities.<sup>22–24</sup> Application of pre-stress can change the phononic properties of solid systems.<sup>25–27</sup> Soft materials can exhibit large deformations<sup>28,29</sup> so that their geometry or even topology can be changed owing to the bulking instability,<sup>30,31</sup> leading to a significant change in wave dispersion. Thermal expansion of a solid material can also be used to control wave propagation to a certain extent.<sup>32</sup> Bistable or multi-steady states of shape memory materials, including shape memory alloys<sup>33</sup> and polymers, can be used for the conversion of different wave characteristics.

Recently, PC slabs have received increasing interest for the manipulation of Lamb waves.<sup>23,34–36</sup> Investigations are focused on flat slabs decorated with holes<sup>37</sup> or solid inclusions<sup>38</sup> or grafted with pillars<sup>39</sup> or resonators.<sup>40</sup> Various devices, such as waveguides,<sup>41</sup> splitters<sup>42</sup> and filters,<sup>43</sup> have been designed and verified experimentally. However, manipulation of Lamb waves remains a difficult task.<sup>23,44,45</sup> In the present work, we demonstrate experimentally a simple way to reconfigure easily waveguides in perforated PC slabs. Threaded rods, held in dry mechanical contact with the slab using nuts, are added at chosen holes. Adjusting the free length of the rods, the resonance frequency of bending modes of the rods can be adjusted continuously within the complete phononic bandgap. Straight waveguides and 90° bent coupled-resonator waveguides are formed experimentally in an aluminum PC slab. To explore the physical mechanism behind waveguiding, numerical simulations by using finite element analysis are performed. Numerical and experimental results generally agree fairly well, with slight frequency shifts of resonances. This work is of significance for the design of reconfigurable elastic wave devices.

## II. EXPERIMENTAL AND NUMERICAL METHODS

The manufactured square-lattice PC slab sample is shown in Fig. 1(a). It is machined in an aluminum plate. It consists of perforated square lumps connected by thin bars. In finite element computations, aluminum is considered isotropic (mass density  $\rho_s = 2700 \text{ kg/m}^3$ , Poisson's ratio  $\nu = 0.33$ , and Young's modulus

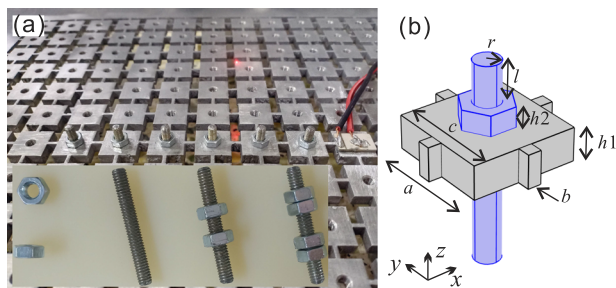


**FIG. 1.** (a) Photograph of the PC slab sample. A linear waveguide is formed by a sequence of threaded rods clamped with nuts to the perforated square lumps. The inset is a close-up view of the rods and nuts used. (b) Unit cell of the PC slab and definition of geometrical dimensions.

$E = 6.89 \text{ GPa}$ ). The lattice constant is  $a = 20 \text{ mm}$ , and the thickness of the slab is  $h_1 = a/4$ . The width of the perforated square lumps is  $c = 0.8a$ , and the width of the connecting bar is  $b = 0.1a$ . The radius of the central hole is  $r = 0.1a$ . With those values, the PC slab possesses a wide complete phononic bandgap, as shown in Fig. 2 (see Sec. III for a discussion).

Reconfigurability is implemented by the addition of threaded steel rods inside selected holes of the PC slab. The rods are clamped to the lumps by steel nuts placed symmetrically on both sides of the plate. The consideration of nuts is not required, in principle. We observed experimentally, however, that the unfastened rods had almost no influence on the transmission properties because the rods are not clamped enough to the PC slab in this case and they can vibrate rather freely. Furthermore, the fastening force applied on each nut was kept sufficiently small to avoid deformations of the supporting PC slab. In numerical computations, steel is considered isotropic (mass density  $\rho_s = 6750 \text{ kg/m}^3$ , Poisson's ratio  $\nu = 0.3$ , and Young's modulus  $E = 206 \text{ GPa}$ ). The thickness of the nuts is  $h_2 = 0.15a$ . The total length of the rods is  $L = 1.5a$  and their radius is  $r = 0.1a$ . As discussed in Sec. III, the effective length of the rod ( $l_e$ ), including both the length from nut to free end ( $l$ ) and the contribution of the nut, defines its resonance frequencies. By symmetry, we need to only consider the length  $l$  of the rod above the plate [see Fig. 1(b)]. The length of the rod below the plate is  $L - h_1 - 2h_2 - l$ .

Lamb waves are excited via a piezoelectric patch. Propagating Lamb waves are detected and imaged using a Polytec PSV-500 scanning vibrometer. Harmonic signals with either stepped or fixed frequencies are chosen for the measurement of transmission and displacement distribution, respectively. The excitation signal is amplified before it is applied to the piezoelectric patch bonded to one side of the slab. The patch is polarized vertically.

Numerical simulations are performed with a 3D finite element method for a better understanding of experimental results and the related physical mechanisms. Band structures are calculated by applying Bloch boundary conditions on the lateral sides of a single unit cell or of a super-cell, depending on the distribution of rods and nuts. Transmission properties are evaluated by considering a finite PC slab, as shown in Fig. 1(a). Note that the pre-stress resulting from the fastening of the nuts is not taken into account in

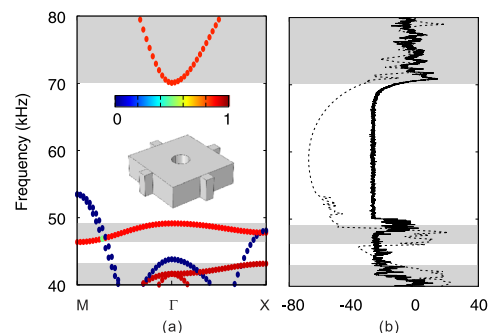


**FIG. 2.** (a) Band structure of the perfect PC slab and (b) transmission properties of the perfect PC obtained from simulation (dashed line) and experiment (solid line). The light-gray parts mark the passing band for out-of-plane modes. The color bar represents the polarization from 0 (blue) to 1 (red).

numerical simulations. An out-of-plane wave source with unit amplitude ( $U_0 = 1$ ) is applied on one side ( $S_1$ ) of the waveguide. By sweeping the frequency, we evaluate the frequency response function (FRF) in decibel units by

$$F(f) = 20 \log_{10} \left( \frac{\int_{S_2} U ds}{\int_{S_1} U_0 ds} \right), \quad (1)$$

where  $U$  is the total displacement collected over a receiver segment ( $S_2$ ) placed at the exit side of the waveguide. It should be noted that both the source and the receiver are located inside the phononic crystal. With this setting, for all frequencies within the complete phononic bandgap, we avoid the interference of guided waves with waves reflecting on the external boundary of the finite structure. To differentiate the polarization of different modes, we further compute the proportion of the out-of-plane displacement in the squared total displacement via

$$p_z = \frac{\int |w|^2 dV}{\int (|u|^2 + |v|^2 + |w|^2) dV}, \quad (2)$$

with  $(u, v, w)$  being the three components of displacement in the reference frame of Fig. 1(b). Experimental and numerical results are compared in detail in Sec. III.

### III. RESULTS AND DISCUSSION

In this section, we discuss the band structures and the frequency response of different phononic circuits.

#### A. Bare phononic crystal slab

For comparison, we first consider the phononic properties of the perfect PC slab summarized in Fig. 2. With the color scale in the phononic band structure varying from in-plane (blue) to out-of-plane polarized (red), it is seen that both polarizations are effectively separated, as results for the mid-plane symmetry of the PC slab. Two bandgaps for out-of-plane Lamb waves are observed in the band structure, covering the frequency ranges between 43.15 and 46.37, and 49.15 and 70.08 kHz. The second, larger, bandgap is mostly considered in the following. The measured frequency response is generally in agreement with the computed band structure and frequency response, though a slight upward frequency shift is observed at the entrance of the bandgap. This difference may be due to the neglect of the presence of threaded holes in the slab, effectively leading to an overestimation of the mass of the perforated lumps. Significantly, the measured bandgap is wide enough for the preparation of different waveguides operating between 50 and 70 kHz, typically.

#### B. Defect modes with rods and nuts

The addition of threaded rods and a pair of nuts allows for the design of reconfigurable waveguides formed from coupled defects. We consider three different values of length  $l$ : (A)  $l = 0$ , (B)  $l = 0.15a$ , and (C)  $l = 0.3a$ . The respective supercells are shown in the first column of Fig. 3. Phononic band structures are shown in the second column of the figure. As a remark, when defects are added, the structure loses the mid-plane symmetry and the separation between

in-plane and out-of-plane polarized elastic waves is lost. It can be seen, however, that bands of the bare PC slab are still apparent with unchanged polarization type. Additionally, defect bands appear. Those have a color in between blue and red, meaning that their polarization is mixed and all three displacements in space coexist. Guiding bands induced by the presence of defect states are identified in dark gray in Fig. 3. Their frequency ranges are reported in Table I.

Vibration modes around 50 kHz for defect A ( $l = 0$ ) are shown in Fig. 3. The bottom free end of the rod vibrates in a bending motion typical of a clamped-free beam. The two modes of vibration depicted are orthogonal and couple with flexural waves of the supporting slab. Since those flexural waves are evanescent in the surrounding PC slab, the defect modes are strongly confined spatially. Globally, one of the pair of modes vibrates in the direction of the waveguide,  $x$ , whereas the other vibrates in the lateral direction,  $y$ . Given the symmetry of the excitation source with respect to the  $x$  axis in the experiment, we expect the latter mode to be deaf and hence not to be excited. In addition, another resonance appears around 65 kHz. This mode is mostly polarized out-of-plane, but there is almost no coupled vibration in the rod. The displacement distribution is asymmetric with respect to the  $x$  axis, so this mode is also expected to be deaf.

When length  $l$  is increased to  $0.15a$  with defect B, the vibration motion remains of the exact same type, but the resonance frequency shifts upward to around 60 kHz. As argued below, the frequency shift results from the decrease in the length of the bottom free end of the rod. When length  $l$  is further increased to  $0.3a$  with defect C, the resonance frequency remains almost the same, around 59 kHz. The top free end of the rod, however, is now vibrating instead of the bottom end.

As observed above, the resonance frequency can be tuned experimentally by adjusting length  $l$ . The dynamic equation for a homogeneous rod according to Euler–Bernoulli beam theory is<sup>46</sup>

$$\frac{\partial^2}{\partial y^2} \left[ EI \frac{\partial^2 v}{\partial y^2} \right] - \rho A \omega^2 v = 0, \quad (3)$$

where  $E$  is Young's modulus,  $I$  is the second moment of area of the beam, and  $A$  is the cross-sectional area. The natural frequency for a clamped-free beam with an effective length  $l_e$  can be evaluated by

$$\omega_n = (\beta_n l_e)^2 (EI/m l_e^4)^{1/2}, \quad (4)$$

where  $n = 1, 2, \dots$  is the order of the vibration mode and  $m = \rho A$  is the mass density per unit length. The numerical value for the mode constants of the first two normal modes are  $(\beta_1 l_e)^2 = 3.5160$  and  $(\beta_2 l_e)^2 = 22.0345$ . For defect C, the resonance can be identified with the first or fundamental normal mode, whereas for defects A and B, the resonance can be identified with the second normal mode. The normal mode frequencies  $\omega_n$  vary with the inverse of the square of the effective length of the rod. It should be stressed, however, that the correspondence is mostly qualitative, since the precise geometry of the nuts is not taken into account in the homogeneous beam model and the clamping boundary condition is only approximately met because of the moderate tightening force that is applied to the nuts. Anyway, this simple model explains the continuous tunability of the resonance frequency by adjustment of the free length of the rod.

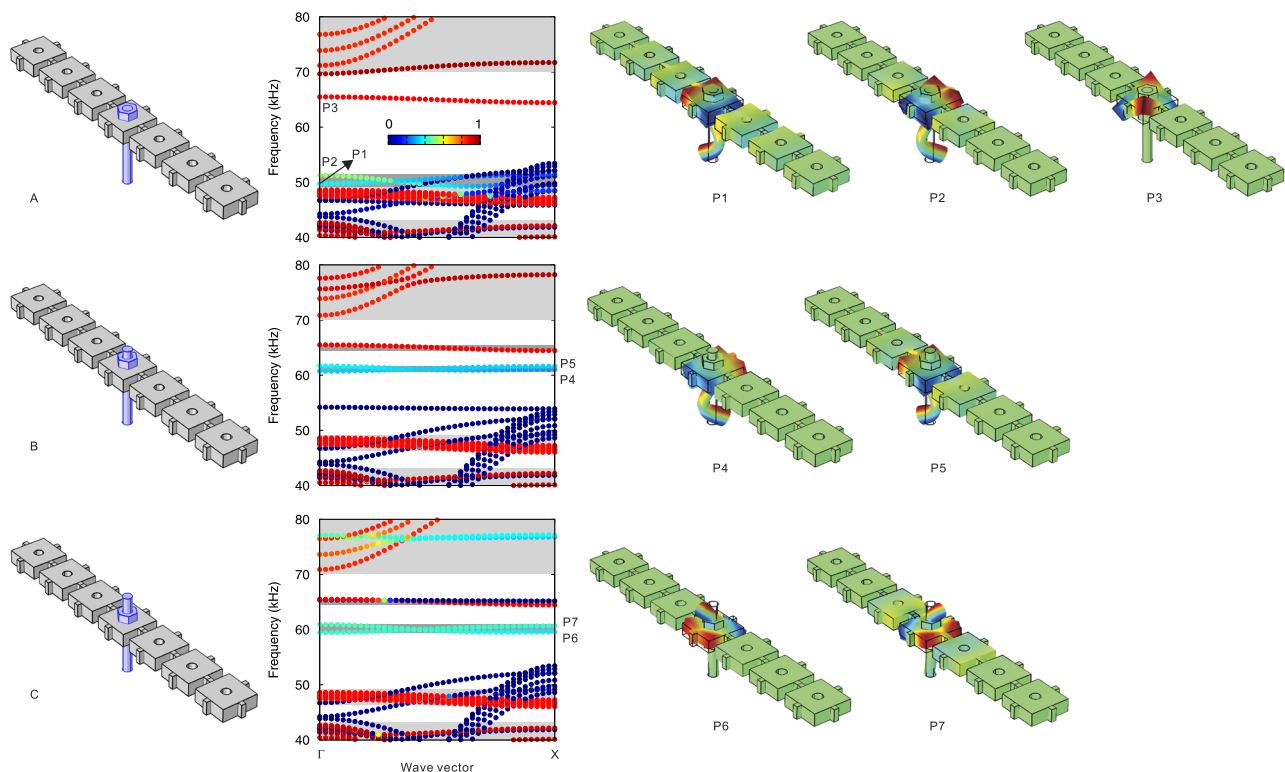


**FIG. 3.** Phononic properties of defects composed of threaded rods held with nuts in the perforated solid PC slab of Fig. 2. Three different defects are introduced, with the varying value of the free length of rod  $l$ : (A)  $l = 0$ , (B)  $l = 0.15a$ , and (C)  $l = 0.3a$ . In each case, the band structure for the corresponding supercell is shown. The color scale represents the contribution of out-of-plane displacements to the total polarization of elastic waves from 0 (blue) to 1 (red). The light-gray areas indicate the passing band for the out-of-plane polarized waves in the perfect PC slab. The dark-gray areas indicate the considered waveguiding bands. Vibration modes at marked points are shown on the right. The color scale represents the normalized amplitude of out-of-plane displacements from negative (blue) to positive (red).

### C. Straight waveguides

In this subsection, we focus on the operation of straight waveguides made from defects A, B, and C. The total length of the straight waveguides is  $6a$  in the experiments, i.e., they are composed of a line of six defects. Numerical and experimental FRFs are shown in Fig. 4. They are in fair agreement but show some differences. For all three defects, the numerical FRF predicts some transmission in a frequency band extending around 65 kHz that is not observed experimentally. From the phononic band structure, this response corresponds to mode P3 in Fig. 3 that should be deaf. The numerical FRF is, however, quite small and may remain below the experimental detection baseline. More significant are the transmission bands

**TABLE I.** Guiding bands predicted from finite element computations and measured for straight and bent waveguides. The frequency unit is kHz.

Type	A	B	C
Numerical	49.3–51.4	60.7–61.7	59.5–61.0
Straight waveguide	52.6–56.0	54.6–63.2	57.6–61.2
Bent waveguide	52.7–55.5	59.0–61.3	60.3–62.0

highlighted in dark gray in Fig. 4. The numerical FRFs clearly correspond to the resonant frequency ranges identified in Fig. 3 and listed in Table I. The experimental FRFs appear to be shifted in frequency compared to their numerical counterparts and to have a wider frequency extension. Since it is known that the frequency bandwidth of coupled-resonator waveguides is directly related to the coupling strength between resonant defects,<sup>47</sup> the observation indicates that coupling may be underestimated in the finite element analysis. Furthermore, clear channeled spectra are observed, with the number of maxima within transmission bands of the order of the number of defects in the coupled chain.<sup>41,48</sup> The frequency shifts of the resonances may be attributed to the difficulty of controlling precisely the pre-stress applied to the nuts in the experimental sample. The pre-stress is assumed to be zero in the numerical simulations. In the experiment, a varying pre-stress is probably applied to each individual defect. The consideration of pre-stress suggests an alternative way of controlling wave propagation in the proposed system and is left for future investigations.

Displacement fields at selected frequencies are measured over the surface and displayed in the rightmost column of Fig. 4. Vibration modes appear to be a combination of the  $x$  and  $y$  polarized modes in Fig. 3. Specifically, modes P1 and P2 degenerate for defect A, modes P4 and P5 degenerate for defect B, and modes P6 and

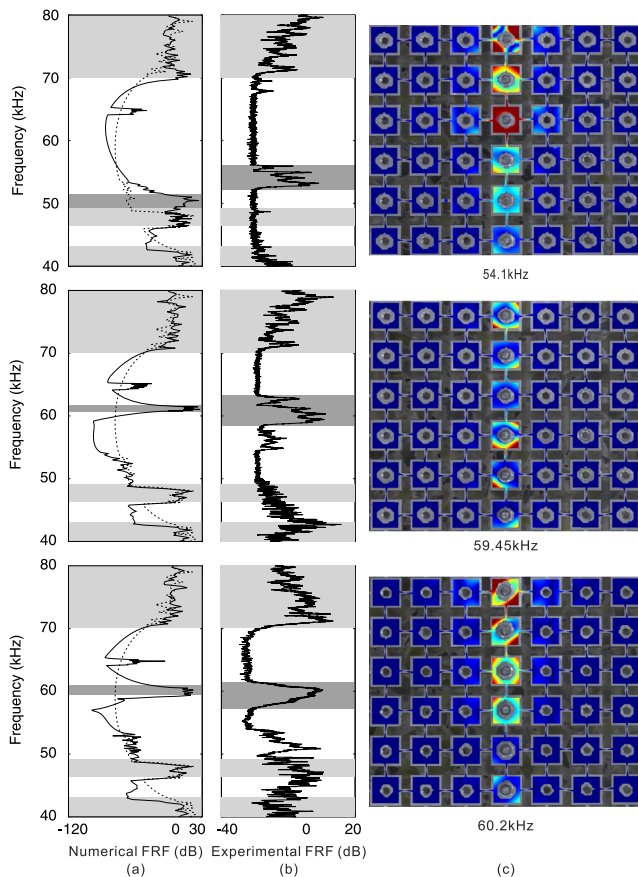


**FIG. 4.** Frequency response function (FRF) of straight waveguides. Numerical and experimental FRFs are shown in panels (a) and (b). The light-gray areas indicate the passing bands for out-of-plane polarized waves in the perfect PC slab. The dark-gray areas indicate the waveguiding bands induced by each defect. The FRF for the bare PC slab is plotted with a dashed line in (a) for comparison. Experimentally measured displacement fields at selected frequencies are displayed in panel (c). The color-scale indicates the amplitude of out-of-plane displacement from 0 (blue) to maximum (red).

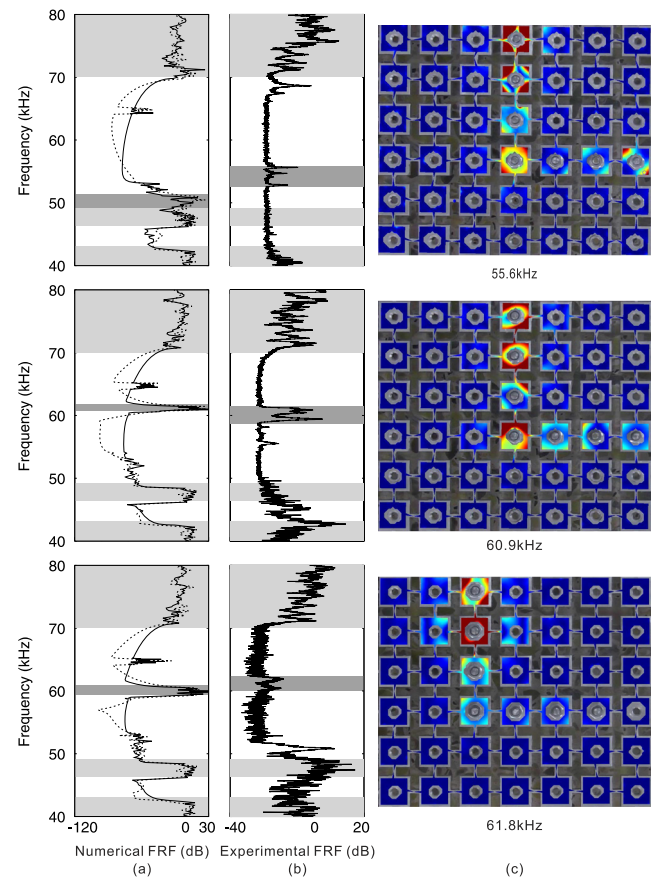


**FIG. 5.** Frequency response function (FRF) of bent waveguides. Numerical and experimental FRFs are shown in panels (a) and (b). The light-gray areas indicate the passing bands for out-of-plane polarized waves in the perfect PC slab. The dark-gray areas indicate the waveguiding bands induced by each defect. The FRFs for the corresponding straight waveguides are plotted with dashed lines in (a) for comparison. Experimentally measured displacement fields at selected frequencies are displayed in panel (c). The color scale indicates the amplitude of out-of-plane displacement from 0 (blue) to maximum (red).

P7 degenerate for defect C. Overall, Lamb waves are clearly guided along the waveguides at different frequencies, thus verifying the reconfigurability of the proposed system. As a note, no attempt was made at adjusting the free length of the rods to match experimental and numerical frequencies.

#### D. Bent waveguides

Beyond straight waveguides, the principle of coupled-resonators also allows one to design more arbitrary chains,<sup>41</sup> whereas for linear or topological waveguides, the angle of bends is restricted by the symmetry of the lattice. The reconfigurability principle, for instance, also applies to 90° bent waveguides for the square lattice, as we consider in this subsection. The total length of the bent waveguides is  $7a$  or a chain of seven coupled defects. Numerical and experimental FRFs are shown in Fig. 5. The numerical FRFs around the resonant bands have limited changes compared to straight waveguides, although bent waveguides have

an additional defect and a sharp band after the fourth defect. Similar observations were made for acoustic waves propagating along linear waveguides.<sup>48</sup> This observation suggests that waveguiding is very efficient in theory and independent of the number of defects as well as of the existence of bends. The experimental FRFs show more changes, especially regarding the width of resonant bands but also the amplitude of the response at the end of the chain of defects.

Displacement fields at selected frequencies are measured over the surface and displayed in the rightmost column of Fig. 5. As in the case of straight waveguides, the mixture of  $x$  and  $y$  polarized modes identified in Fig. 3 explains how Lamb waves are guided along the chain of defects, especially across the 90° bend.

#### IV. CONCLUSION

In this paper, Lamb wave propagation in phononic circuits formed by reconfigurable chains of defects has been investigated.

Defects are introduced by attaching threaded rods with nuts to a two-dimensional perforated square-lattice PC slab. The consideration of threaded rods naturally provides reconfigurability by adjusting continuously their free length and hence their natural resonance frequencies. In addition, the solid PC slab is completely reusable and unaltered when reconfiguring the phononic circuits. Both straight and 90° bent waveguides were designed and fabricated. As illustrated by a simple bending cantilever model, the central frequency can span the available complete phononic bandgap. In numerical simulations, the frequency response function is almost independent of the length of the chain of defects and of the presence of bends. Experimental results are generally in fair agreement with numerical ones, although the mechanical reconfigurability provided by a human experimenter remains somehow imprecise, including the pre-stress applied when fastening the nuts. Mechanical robots with force sensors may be considered to conduct precise control of wave propagation. Other phononic circuits could also be designed as a direct extension of the present work.

## ACKNOWLEDGMENTS

The authors acknowledge Wei Guo's assistance for additional experiments performed during the revision of the manuscript. Financial support from the National Natural Science Foundation of China (Grant Nos. 12072223, 12021002, 11991031, and 11991032) is gratefully acknowledged. Y.F.W. acknowledges support from the National Science Foundation of Tianjin (Grant No. 20JCQNJC01030). V.L. acknowledges support from the EIPHI Graduate School (Contract No. "ANR-17-EURE-0002").

## DATA AVAILABILITY

The data that support the findings of this study are available from the corresponding author upon reasonable request.

## REFERENCES

- M. S. Kushwaha, P. Halevi, L. Dobrzynski, and B. Djafari-Rouhani, "Acoustic band structure of periodic elastic composites," *Phys. Rev. Lett.* **71**, 2022 (1993).
- M. B. Assouar, M. Senesi, M. Oudich, M. Ruzzene, and Z. Hou, "Broadband plate-type acoustic metamaterial for low-frequency sound attenuation," *Appl. Phys. Lett.* **101**, 173505 (2012).
- A. Khelif, A. Choujaa, S. Benchabane, B. Djafari-Rouhani, and V. Laude, "Guiding and bending of acoustic waves in highly confined phononic crystal waveguides," *Appl. Phys. Lett.* **84**, 4400 (2004).
- Y. Pennec, B. Djafari-Rouhani, J. O. Vasseur, A. Khelif, and P. A. Deymier, "Tunable filtering and demultiplexing in phononic crystals with hollow cylinders," *Phys. Rev. E* **69**, 046608 (2004).
- Y. Pennec, B. Djafari-Rouhani, J. O. Vasseur, H. Larabi, A. Khelif, A. Choujaa, S. Benchabane, and V. Laude, "Acoustic channel drop tunneling in a phononic crystal," *Appl. Phys. Lett.* **87**, 261912 (2005).
- M. I. Hussein, M. J. Leamy, and M. Ruzzene, "Dynamics of phononic materials and structures: Historical origins, recent progress, and future outlook," *Appl. Mech. Rev.* **66**, 040802 (2014).
- Y.-F. Wang, Y.-Z. Wang, B. Wu, W. Chen, and Y.-S. Wang, "Tunable and active phononic crystals and metamaterials," *Appl. Mech. Rev.* **72**, 040801 (2020).
- V. Laude, *Phononic Crystals: Artificial Crystals for Sonic, Acoustic, and Elastic Waves* (Walter de Gruyter GmbH, Berlin, 2015).
- R. Zhu, Y. Y. Chen, M. V. Barnhart, G. K. Hu, C. T. Sun, and G. L. Huang, "Experimental study of an adaptive elastic metamaterial controlled by electric circuits," *Appl. Phys. Lett.* **108**, 011905 (2016).
- N. Kherraz, L. Haumesser, F. Levassort, P. Benard, and B. Morvan, "Controlling Bragg gaps induced by electric boundary conditions in phononic piezoelectric plates," *Appl. Phys. Lett.* **108**, 093503 (2016).
- N. Kherraz, L. Haumesser, F. Levassort, P. Benard, and B. Morvan, "Hybridization bandgap induced by an electrical resonance in piezoelectric metamaterial plates," *J. Appl. Phys.* **123**, 094901 (2018).
- K. L. Jim, C. W. Leung, S. T. Lau, S. H. Choy, and H. L. W. Chan, "Thermal tuning of phononic bandstructure in ferroelectric ceramic/epoxy phononic crystal," *Appl. Phys. Lett.* **94**, 193501 (2009).
- J.-F. Robillard, O. B. Matar, J. O. Vasseur, P. A. Deymier, M. Stippinger, A.-C. Hladky-Hennion, Y. Pennec, and B. Djafari-Rouhani, "Tunable magnetoelastic phononic crystals," *Appl. Phys. Lett.* **95**, 124104 (2009).
- S. Xiao, G. Ma, Y. Li, Z. Yang, and P. Sheng, "Active control of membrane-type acoustic metamaterial by electric field," *Appl. Phys. Lett.* **106**, 091904 (2015).
- A. Bergamini, T. Delpero, L. De Simoni, L. Di Lillo, M. Ruzzene, and P. Ermanni, "Phononic crystal with adaptive connectivity," *Adv. Mater.* **26**, 1343–1347 (2014).
- W. Qian, Z. Yu, X. Wang, Y. Lai, and B. B. Yellen, "Elastic metamaterial beam with remotely tunable stiffness," *J. Appl. Phys.* **119**, 055102 (2016).
- O. R. Bilal, A. Foehr, and C. Daraio, "Reprogrammable phononic metasurfaces," *Adv. Mater.* **29**, 1700628 (2017).
- J. Hwan Oh, I. Kyu Lee, P. Sik Ma, and Y. Young Kim, "Active wave-guiding of piezoelectric phononic crystals," *Appl. Phys. Lett.* **99**, 083505 (2011).
- Y.-Z. Wang, F.-M. Li, and Y.-S. Wang, "Active feedback control of elastic wave metamaterials," *J. Intell. Mater. Syst. Struct.* **28**, 2110 (2017).
- F. Casadei, T. Delpero, A. Bergamini, P. Ermanni, and M. Ruzzene, "Piezoelectric resonator arrays for tunable acoustic waveguides and metamaterials," *J. Appl. Phys.* **112**, 064902 (2012).
- H. Pichard, O. Richoux, and J.-P. Groby, "Experimental demonstrations in audible frequency range of band gap tunability and negative refraction in two-dimensional sonic crystal," *J. Acoust. Soc. Am.* **132**, 2816 (2012).
- Y. Jin, Y. Pennec, Y. Pan, and B. Djafari-Rouhani, "Phononic crystal plate with hollow pillars actively controlled by fluid filling," *Crystals* **6**, 64 (2016).
- T.-T. Wang, Y.-F. Wang, Y.-S. Wang, and V. Laude, "Tunable fluid-filled phononic meta-strip," *Appl. Phys. Lett.* **111**, 041906 (2017).
- Y.-F. Wang, T.-T. Wang, Y.-S. Wang, and V. Laude, "Reconfigurable phononic crystal circuits formed by coupled acoustoelastic resonators," *Phys. Rev. Appl.* **8**, 014006 (2017).
- B. Dubuc, A. Ebrahimkhanlou, and S. Salamone, "The effect of applied stress on the phase and group velocity of guided waves in anisotropic plates," *J. Acoust. Soc. Am.* **142**, 3553 (2017).
- M. Mazzotti, I. Bartoli, and M. Miniaci, "Modelling Bloch waves in prestressed phononic crystal plates," *Front. Mater.* **6**, 74 (2019).
- M. Miniaci, M. Mazzotti, A. Amendola, and F. Fraternali, "Effect of prestress on phononic band gaps induced by inertial amplification," *Int. J. Solids Struct.* **216**, 156–166 (2021).
- T. Mullin, S. Deschanel, K. Bertoldi, and M. C. Boyce, "Pattern transformation triggered by deformation," *Phys. Rev. Lett.* **99**, 084301 (2007).
- B. Li, Y.-P. Cao, X.-Q. Feng, and H. Gao, "Mechanics of morphological instabilities and surface wrinkling in soft materials: A review," *Soft Matter* **8**, 5728 (2012).
- P. Wang, F. Casadei, S. Shan, J. C. Weaver, and K. Bertoldi, "Harnessing buckling to design tunable locally resonant acoustic metamaterials," *Phys. Rev. Lett.* **113**, 014301 (2014).
- S. Shan, S. H. Kang, P. Wang, C. Qu, S. Shian, E. R. Chen, and K. Bertoldi, "Harnessing multiple folding mechanisms in soft periodic structures for tunable control of elastic waves," *Adv. Funct. Mater.* **24**, 4935 (2014).
- A. Bayat and F. Gordaninejad, "A thermally tunable phononic crystal," *Proc. SPIE* **9800**, 98000W (2016).
- M. Ruzzene and A. Baz, "Control of wave propagation in periodic composite rods using shape memory inserts," *J. Vib. Acoust.* **122**, 151 (2000).
- T.-T. Wu, J.-C. Hsu, and J.-H. Sun, "Phononic plate waves," *IEEE Trans. Ultrason., Ferroelectr., Freq. Control* **58**, 2146–2161 (2011).
- A. Climente, D. Torrent, and J. Sánchez-Dehesa, "Gradient index lenses for flexural waves based on thickness variations," *Appl. Phys. Lett.* **105**, 064101 (2014).

- <sup>36</sup>M. Miniaci, A. Marzani, N. Testoni, and L. De Marchi, "Complete band gaps in a polyvinyl chloride (PVC) phononic plate with cross-like holes: Numerical design and experimental verification," *Ultrasonics* **56**, 251–259 (2015).
- <sup>37</sup>Y.-F. Wang and Y.-S. Wang, "Multiple wide complete bandgaps of two-dimensional phononic crystal slabs with cross-like holes," *J. Sound Vib.* **332**, 2019–2037 (2013).
- <sup>38</sup>F. L. Hsiao, A. Khelif, H. Moubchir, A. Choujaa, C. C. Chen, and V. Laude, "Waveguiding inside the complete band gap of a phononic crystal slab," *Phys. Rev. E* **76**, 056601 (2007).
- <sup>39</sup>M. Oudich, M. B. Assouar, and Z. Hou, "Propagation of acoustic waves and waveguiding in a two-dimensional locally resonant phononic crystal plate," *Appl. Phys. Lett.* **97**, 193503 (2010).
- <sup>40</sup>Y. Xiao, J. Wen, and X. Wen, "Flexural wave band gaps in locally resonant thin plates with periodically attached spring-mass resonators," *J. Phys. D: Appl. Phys.* **45**, 195401 (2012).
- <sup>41</sup>T.-T. Wang, S. Bargiel, F. Lardet-Vieudrin, Y.-F. Wang, Y.-S. Wang, and V. Laude, "Collective resonances of a chain of coupled phononic microresonators," *Phys. Rev. Appl.* **13**, 014022 (2020).
- <sup>42</sup>Y.-F. Wang, T.-T. Wang, J.-P. Liu, Y.-S. Wang, and V. Laude, "Guiding and splitting Lamb waves in coupled-resonator elastic waveguides," *Compos. Struct.* **206**, 588–593 (2018).
- <sup>43</sup>H. Zhu and F. Semperlotti, "Metamaterial based embedded acoustic filters for structural applications," *AIP Adv.* **3**, 092121 (2013).
- <sup>44</sup>M. Miniaci, R. K. Pal, B. Morvan, and M. Ruzzene, "Experimental observation of topologically protected helical edge modes in patterned elastic plates," *Phys. Rev. X* **8**, 031074 (2018).
- <sup>45</sup>M. Miniaci, R. K. Pal, R. Manna, and M. Ruzzene, "Valley-based splitting of topologically protected helical waves in elastic plates," *Phys. Rev. B* **100**, 024304 (2019).
- <sup>46</sup>W. T. Thomson, *Theory of Vibration with Application* (Prentice-Hall, NJ, 1983).
- <sup>47</sup>J. M. Escalante, A. Martínez, and V. Laude, "Dispersion relation of coupled-resonator acoustic waveguides formed by defect cavities in a phononic crystal," *J. Phys. D: Appl. Phys.* **46**, 475301 (2013).
- <sup>48</sup>Y.-F. Wang, T.-T. Wang, J.-W. Liang, Y.-S. Wang, and V. Laude, "Channeled spectrum in the transmission of phononic crystal waveguides," *J. Sound Vib.* **437**, 410–421 (2018).